Optics Letters

Single-shot reconstruction of spectral amplitude and phase in a fiber ring cavity at a 80 MHz repetition rate

Jonas Hammer,[1] P. Hosseini,[1] C. R. Menyuk,[2] Philip St.J. Russell,[1,3] and Nicolas Y. Joly[1,3,*]

[1]Max-Planck Institute for the Science of Light, Guenther-Scharowsky Str. 1, 91058 Erlangen, Germany
[2]University of Maryland, Baltimore County, 1000 Hilltop Circle, Baltimore, Maryland 21250, USA
[3]University of Erlangen-Nuremberg, Guenther-Scharowsky Str. 1, 91058 Erlangen, Germany
*Corresponding author: nicolas.joly@mpl.mpg.de

Received 27 July 2016; revised 9 September 2016; accepted 9 September 2016; posted 12 September 2016 (Doc. ID 272502); published 3 October 2016

Femtosecond pulses circulating in a synchronously driven fiber ring cavity have complex amplitude and phase profiles that can change completely from one round-trip to the next. We use a recently developed technique, combining dispersive Fourier transformation) with spectral interferometry, to reconstruct the spectral amplitude and phase at each round-trip and, thereby, follow in detail the pulse reorganization that occurs. We focus on two different regimes: a period-two regime in which the pulse alternates between two distinct states and a highly complex regime. We characterize the spectral amplitude and phase of the pulses in both regimes at a repetition rate of 75.6 MHz and find good agreement with modeling of the system based on numerical solutions of the generalized nonlinear Schrödinger equation with feedback.

OCIS codes: (320.7100) Ultrafast measurements; (120.5050) Phase measurement; (060.5295) Photonic crystal fibers; (190.3100) Instabilities and chaos.

http://dx.doi.org/10.1364/OL.41.004641

Passive ring cavities [1] have attracted renewed interest in recent years [2–7], being applied for example, to noise reduction in supercontinuum (SC) generation [2], the tailoring of SC spectra [3,4], and frequency comb generation [5]. They can also exhibit complex shot-to-shot dynamics, ranging from period doubling to chaos [1,6,7], which is of interest in applications such as secure telecommunications [8,9]. A fundamental understanding of the underlying processes that drive the observed dynamics, however, has been significantly hindered by a lack of information on how a cavity pulse changes from one round-trip to the next. Although some insight can be gained from numerical simulations [3–5,7], validation requires experimental access to the amplitude and phase of the pulse. Here we report the use of the dispersive Fourier transformation (DFT) [10,11], combined with Fourier transform spectral interferometry (FTSI) [12,13], to characterize the pulses [14] at the output of a synchronously pumped ring cavity operating at a 75.6 MHz repetition rate [6,7]. Pulse reconstruction at such high rates is impossible using schemes based on charge-coupled devices (e.g., GRENOUILLE or SPIDER [15]) because of their slow (ms) response times [16].

The DFT is a spectro-temporal analogue to Fraunhofer diffraction. It uses group velocity dispersion to map the spectral features of a pulse into the temporal domain, allowing them to be monitored using a fast oscilloscope at repetition rates much higher than is possible with conventional spectral techniques. DFT was originally proposed for measurement of fiber dispersion [10] and, since then, has been used in a variety of contexts such as the study of the coherence in supercontinuum generation [17], the characterization of coherent synchrotron radiation [18] and, just recently, for observing the onset of mode-locking in a Ti:sapphire oscillator [19]. It has also been shown that two independent DFT measurements can be used to retrieve phase information [20].

In this Letter, we use a combination of DFT and FTSI to measure single-shot spectra and spectral phases at a repetition rate of 75.6 MHz. This approach requires a stable reference pulse with a bandwidth at least as wide as the pulses under study. The reference pulse is generated in a specially designed all-normal-dispersion [21] photonic crystal fiber (PCF), referred to as the broadening fiber (BF). An electron micrograph of its microstructure is shown in Fig. 1; the diameter of the hollow channels is 0.53 μm, and the inter-channel spacing is 1.42 μm. The resulting dispersion curve, calculated using the empirical model of Saitoh and Koshiba [22], is plotted in Fig. 1(a). Since the broadening mechanism in the BF is self-phase modulation [Fig. 1(b)], an input pulse not only broadens spectrally as it propagates, but also acquires a parabolic, smooth and low-noise phase profile [23,24]—features that are of great importance for reliable phase retrieval.

Spectral interferometry is a linear technique suitable for retrieving phase information from two overlapping light pulses [25,26]. To retrieve the spectral phase of the pulse under study, we use a Mach–Zehnder interferometer (MZI) to overlap a reference pulse (which has a known phase) with the pulse under

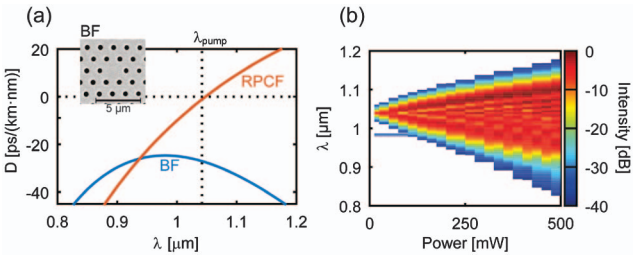

Fig. 1. (a) Dispersion of the spectral BF and the ring-PCF (RPCF). The inset shows a scanning electron micrograph of the BF structure. (b) Measured power dependence of the spectrum at the output of the BF. The line at ∼980 nm is residual CW pump light from the Yb-doped laser. It does not contribute to the ring cavity dynamics.

study. If τ is the time delay between the two pulses, $S_0(\omega)$ is the spectrum of the reference pulse, $S(\omega)$ is the spectrum of the pulse under study, and $\varphi_0(\omega)$ and $\varphi(\omega)$ are the respective spectral phases, we can write the combined spectrum at the output of the MZI as

$$S_{\mathrm{MZI}}(\omega) = S_0(\omega) + S(\omega) + 2\sqrt{S_0(\omega)S(\omega)}\cos[\phi_0(\omega) - \phi(\omega) - \omega\tau]. \quad \textbf{(1)}$$

Using FTSI, we can use Eq. (1) to extract phase information of the pulse under study, provided the amplitude and phase of the reference pulse are known [13]. For this purpose, we used a frequency-resolved optical gating (FROG) device to characterize the reference pulse.

The ring cavity is placed in one arm of the MZI (Fig. 2); the second arm contains the BF to generate the reference. The output of the MZI is monitored either by an optical spectrum analyzer (OSA) or by a DFT setup consisting of 2 km of dispersive fiber (Corning HI1060 Flex) and a 12 GHz photodiode (PD2) connected to a 6 GHz oscilloscope. The dispersion of the fiber that is used for the DFT is $\beta_2 = 31\ \mathrm{ps^2\,km^{-1}}$, so that the limit

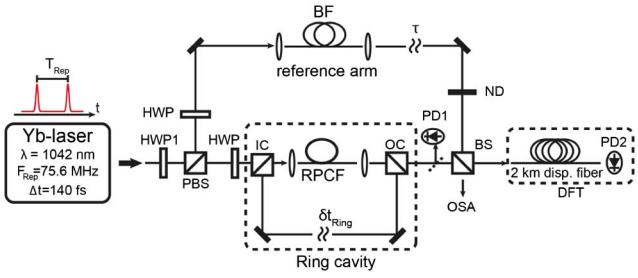

Fig. 2. Experimental setup. The polarization state is adjusted with half-wave plates. The Mach–Zehnder interferometer is terminated by a polarization beam splitter at the entrance and a 50:50 beam splitter at the output. Photodiode 1 (PD1, 2 GHz) registers the shot-to-shot energies of the pulses exiting the ring cavity and triggers the DFT measurement. In the reference arm, the all-normal-dispersion PCF (BF) is ∼5 cm long, and the pulses from the BF are attenuated with a variable ND filter. A delay τ adjusts the overlap between the pulses traveling in the arms of the MZI. The output of the DFT is monitored with a 12 GHz photodiode PD2 connected to a 6 GHz oscilloscope. The ring cavity consists of a PCF (RPCF) embedded inside an optical feedback loop terminated by two beam splitters with fixed reflectivity (IC 90% and OC 99%). A delay δt_{ring} adjusts the temporal overlap between the circulating pulse and the pump.

on the spectral resolution due to the finite fiber length is given by $\Delta\lambda = \lambda^2 c^{-1}(\pi\beta_2 L_{\mathrm{DFT}})^{-1/2} = 0.26$ nm [11]. We estimate the actual resolution to be 1.4 nm, as a result of the limited response time of PD2-plus-oscilloscope. The fringe visibility at the output of the MZI was optimized by adjusting the pulse energy in the reference arm using a variable neutral density (ND) filter after BF, and by adjusting the polarization state in the reference arm.

A mode-locked Yb-doped laser operating at 1042 nm delivered pulses of bandwidth 10 nm at 75.6 MHz with a maximum average power of 500 mW. Upon entering the ring cavity, the pulses had a slight positive chirp. The ring cavity consisted of a photonic crystal fiber (labeled RPCF) with a zero dispersion wavelength of 1058 nm, as shown in Fig. 1(a). By adjusting the temporal walk-off between the pulse traveling in the ring cavity and the pump pulse, a variety of regimes with complex nonlinear dynamics could be observed, for example, steady-state and period-two, in which the pulse energy alternates between two distinct values. More complex states could also be observed [6,7].

The phase-retrieval system was first calibrated by blocking the optical feedback to the ring cavity, i.e., pulses passed through the RPCF only once. We coupled 30 mW into the BF and 25 mW into the RPCF. At the exit from the BF, the pulses were ∼340 fs long with a spectrum extending from 1020 to 1060 nm (10 dB level) relative to the maximum power. The delay τ between the pulses from the BF and the RPCF was set to 900 fs, so as to fulfill the criterion for FTSI [13]. The spectral interference of the overlapping pulses was measured by both the DFT and the OSA, as shown in Fig. 3(a). The wavelength axis of the DFT was calibrated by identifying spectral features in traces recorded by both the DFT and the OSA, as shown in the inset of Fig. 3(a). The seemingly low visibility of the fringes in the DFT trace is due to the convolution of the output signal with the photodiode and oscilloscope response function. For reconstruction of the unknown power spectrum, the corresponding DFT traces were deconvolved by dividing the Fourier transform of the DFT trace by the frequency response of the photodiode. We reduce the artificial amplification of the noise by numerically filtering the high-frequency components of the deconvolved trace. The resulting spectra agree well with those measured by the OSA. Empirically, we found that this deconvolution process does not affect the spectral phase information. We chose to work with the original signal for phase retrieval and used the deconvolution for reconstruction of the power spectra.

From the measured spectral interference at the output of the MZI, the spectral phase of the pulses exiting the RPCF could be retrieved using FTSI. Following [27], we calibrated the FTSI system and checked it against FROG measurements. Good agreement was obtained. In Fig. 3(b), we show single-shot phase measurements evenly distributed over the full period of 1500 pulses. The results are self-consistent over the full duration of the recording (1500 pulses in 20 μs).

We next investigated a periodic state of the ring cavity for a power of 17 mW, coupled into the RPCF. The temporal walk-off δt_{ring} was adjusted so that the temporal energy profile of the pulses exiting the cavity evolved in a period-two regime [6], i.e., when the output energy recorded at PD1 alternates between two distinct values [28], as shown in Figs. 4(a) and 4(b), Fig. 4(b) is a first-return diagram, which conveniently

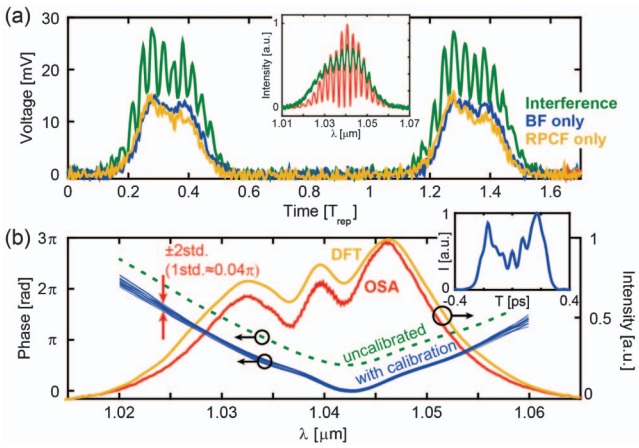

Fig. 3. (a) DFT traces recorded by PD2, corresponding to the spectra of two successive pulses. The time axis is normalized to the laser repetition rate T_{rep}. Yellow, the RPCF signal; blue, the BF signal; green, the interference of the two signals. The inset compares the wavelength-calibrated DFT measurement of the interference (green) with the same signal recorded by the OSA (red); the green curve is a superposition of 10 single-shot measurements. (b) Red, spectrum of RPCF signal measured with the OSA; yellow, averaged spectrum measured with DFT after deconvolution; green, average over 1500 single-shot phase measurements of RPCF in a single-pass configuration with DFT+FTSI before the calibration described in the text; the curve is shifted upward for clarity. Blue, 15 single-shot phase measurements after calibration, corresponding to every tenth pulse from the measurement. A standard deviation of $\sim 0.04\pi$ is estimated from 1500 consecutive pulses. The inset in (b) shows the averaged intensity profile of the pulse in the time domain.

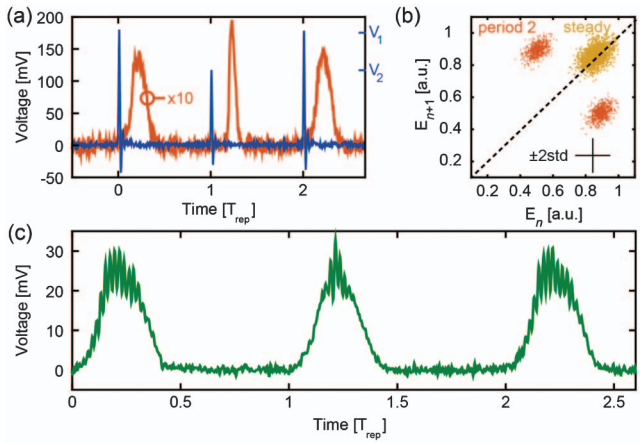

Fig. 4. (a) Solid blue, three consecutive pulses from the ring cavity, recorded by PD1. The peak height is proportional to the pulse energy and is found to alternate between two distinct states (V1 and V2). Solid orange, corresponding spectra recorded by PD2 at the output of the DFT (scaled up by a factor of 10); the spectrum alternates in line with the pulse energy. (b) First-return diagram of the pulse energy calculated by integrating the spectra, which plots the energy of pulse n versus that of pulse $n+1$. The yellow region shows the noise level in the steady state, and the orange region shows the period-two state. (c) A DFT-MZI measurement of the two states by interference with the reference pulses.

represents complex time sequences in dynamical systems [29]. The corresponding DFT trace confirms that the pulse spectrum alternates between two distinct states, each state repeating itself at every other round-trip. This behavior is hidden if an OSA or a CCD spectrometer is used because such spectral measurement systems respond too slowly to follow the shot-to-shot evolution at high repetition rates (75.6 MHz, in this case). Additionally, since the output from the reference arm remains constant, the spectrum (amplitude and phase) of each state can be retrieved using the FTSI algorithm with single-shot DFT data. Fig. 4(c) shows part of the DFT trace in which the output of the ring cavity interferes with the output of the BF. The spectral phases of 20 pulses, randomly chosen from the whole duration of the measurement, are shown in Fig. 5(a). They are found to alternate between two states of similar functional shape, shifted by $\sim 0.3\pi$, which is about three times more than the standard deviation for both states. We performed simulations based on solving the generalized nonlinear Schrödinger equation (GNLSE), including feedback [6,23], using the experimentally measured pulse from the laser as the pump. The overall positive chirp that we can record is linked to the initial phase profile of the pulse. For $\delta t_{ring} = -3.4$ fs, the simulations show period-two states with similar spectral shapes and a comparable phase shift between those states. Even though the GNLSE is not sensitive to the constant phase on the input pulse, the modeling is still sensitive to sub-cycle changes in temporal walk-off, reflecting the experimentally observed complexity of the system's behavior. This sensitivity implies that interference at the coupling beam splitter plays a major role in the overall dynamics of the system, since it yields different initial conditions for the pulse entering the fiber at each round-trip. The time-domain pulses calculated from the measurement and simulation are shown as insets in Fig. 5. Although the simulated pulse shows more fine structure than the measured pulse, the overall shape is similar. The pulse from the spectrally

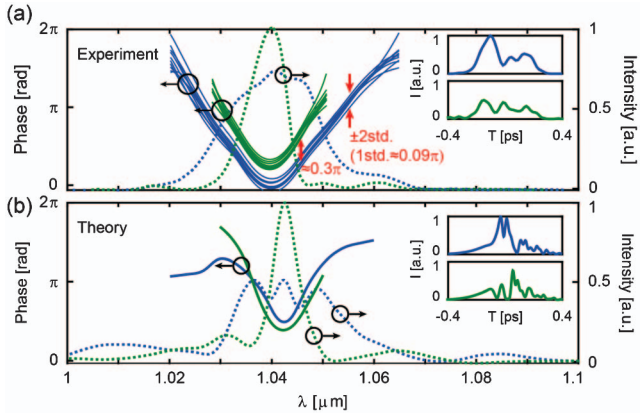

Fig. 5. (a) Dashed green and blue, power spectra of both states averaged over 750 measurements each after the deconvolution process. Solid green and blue, single-shot phase measurements for both states. The 10 lines for each state correspond to 10 measurements evenly distributed over the total of 750 measured phases per state. The standard deviation is about 0.09π for the whole set of phases. (b) Simulation of a period-two state for similar conditions as those in the experiment. Two distinct power spectra can be distinguished, and the characteristic phase jump can be observed. The insets in (a) and (b) show the averaged time-domain pulse in the experiment and the simulation, respectively.

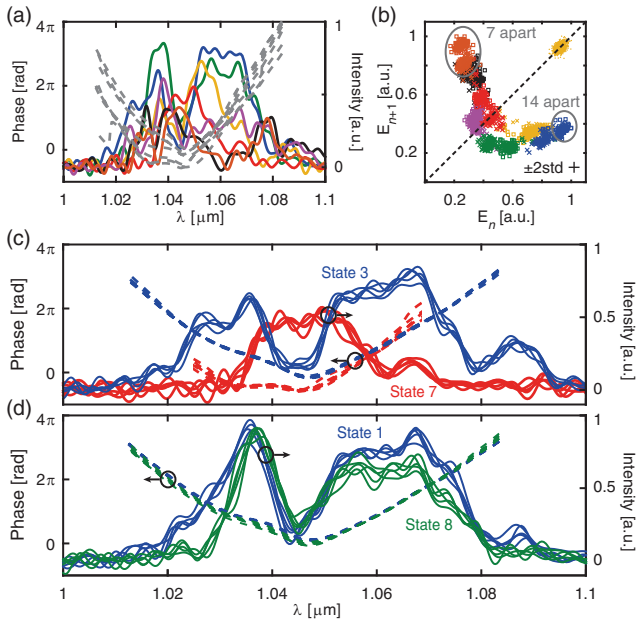

Fig. 6. (a) Seven consecutive spectra and spectral phases (gray) from a highly complex state. The pulse spectrum n has the same color as the corresponding entry (E_n, E_{n+1}) in (b). (b) First-return diagram of pulse energy in this state. In the main band, the seven colors repeat at every seventh round-trip, whereas each unique combination of color and marker (squares or x's) repeats every fourteenth round-trip. The yellow region (top right) shows for comparison the first-return diagram for the system in a steady state and illustrates the noise level. (c) Spectra and spectral phases for two different states in the complex regime; colors correspond to those in (b). (d) Spectra and spectral phases for two different states that are separated by exactly seven pulses.

broader state is divided into a main lobe and trailing satellites, while the pulse from the narrow state consists of multiple similar-sized lobes.

Finally, we studied a highly complex train of pulses where spectrum and energy change on every round-trip, as shown in Figs. 6(a) and 6(b). On the first-return diagram, the seven colored regions repeat every seventh round-trip, whereas each unique combination of color and marker (squares or x's) repeats every fourteenth round-trip. This reveals a period-14 state in which the nth and $(n+7)$th repetitions are very similar. From this result, we infer that the system was close to a bifurcation. A closer look at the two spectra in Fig. 6(d) reveals that two states exactly seven pulses apart do indeed look very similar. A comparison of two states that are not separated by seven repetitions, seen in Fig. 6(c), shows strong spectral reorganization. A phase shift around the central wavelength can be observed that is similar to that seen in the period-two state. The phase shifts between successive pulses do not seem to follow any particular pattern. Note also that the spectral phases in this state are not only shifted, but also can have a different functional shape, as seen in Fig. 6(c).

In conclusion, DFT-FTSI can be used to investigate the dynamics of a passive ring cavity pumped by fs-pulses at a repetition rate of 75.6 MHz. Simulations based on solutions of the GNLSE reproduce the experimental observations and suggest that the driving mechanism for the complex behavior of the system is interference at the coupling beam splitter. Although the traveling pulse can change on every pass in the ring cavity, the shot-to-shot coherence is not lost, as is confirmed in the experiments by the persistently good visibility of the fringes that result from the overlap of two consecutive pulses.

Acknowledgment. The work of C. R. Menyuk was carried out in part while he was a guest at the Max-Planck Institute for the Science of Light, with support from the Alexander von Humboldt Foundation. The authors thank S. Bielawski and C. Szwaj for fruitful discussions.

REFERENCES AND NOTES

1. K. Ikeda, Opt. Commun. **30**, 257 (1979).
2. N. Brauckmann, M. Kues, P. Groß, and C. Fallnich, Opt. Express **19**, 14763 (2011).
3. M. Tlidi, A. Mussot, E. Louvergneaux, G. Kozyreff, A. G. Vladimirov, and M. Taki, Opt. Lett. **32**, 662 (2007).
4. N. Brauckmann, M. Kues, P. Groß, and C. Fallnich, Opt. Express **18**, 20667 (2010).
5. S. Coen, H. G. Randle, T. Sylvestre, and M. Erkintalo, Opt. Lett. **38**, 37 (2013).
6. M. J. Schmidberger, W. Chang, P. St.J. Russell, and N. Y. Joly, Opt. Lett. **37**, 3576 (2012).
7. M. J. Schmidberger, D. Novoa, F. Biancalana, P. St.J. Russell, and N. Y. Joly, Opt. Express **22**, 3045 (2014).
8. A. Argyris, D. Syvridis, L. Larger, V. Annovazzi-Lodi, P. Colet, I. Fischer, J. Garcia-Ojalvo, C. R. Mirasso, L. Pesquera, and K. A. Shore, Nature **438**, 343 (2005).
9. R. Lavrov, M. Peil, M. Jacquot, L. Larger, V. Udaltsov, and J. Dudley, Phys. Rev. E **80**, 026207 (2009).
10. Y. Tong, L. Chan, and H. Tsang, Electron. Lett. **33**, 983 (1997).
11. K. Goda, D. R. Solli, K. K. Tsia, and B. Jalali, Phys. Rev. A **80**, 043821 (2009).
12. M. Takeda, H. Ina, and S. Kobayash, J. Opt. Soc. Am. **72**, 156 (1982).
13. L. Lepetit, G. Chériaux, and M. Joffre, J. Opt. Soc. Am. B **12**, 2467 (1995).
14. M. H. Asghari, Y. Park, and J. Azaña, Opt. Express **18**, 16526 (2010).
15. I. A. Walmsley and C. Dorrer, Adv. Opt. Photon. **1**, 308 (2009).
16. W. Kornelis, J. Biegert, J. W. G. Tisch, M. Nisoli, G. Sansone, C. Vozzi, S. D. Silvestri, and U. Keller, Opt. Lett. **28**, 281 (2003).
17. B. Wetzel, A. Stefani, L. Larger, P. A. Lacourt, J. M. Merolla, T. Sylvestre, A. Kudlinski, A. Mussot, G. Genty, F. Dias, and J. M. Dudley, Sci. Rep. **2**, 882 (2012).
18. E. Roussel, C. Evain, M. L. Parquier, C. Szwaj, S. Bielawski, L. Manceron, J.-B. Brubach, M.-A. Tordeux, J.-P. Ricaud, L. Cassinari, M. Labat, M. E. Couprie, and P. Roy, Sci. Rep. **5**, 10330 (2015).
19. G. Herink, B. Jalali, C. Ropers, and D. R. Solli, Nat. Photonics **10**, 321 (2016).
20. D. R. Solli, S. Gupta, and B. Jalali, Appl. Phys. Lett. **95**, 231108 (2009).
21. A. M. Heidt, A. Hartung, G. W. Bosman, P. Krok, E. G. Rohwer, H. Schwoerer, and H. Bartelt, Opt. Express **19**, 3775 (2011).
22. K. Saitoh and M. Koshiba, Opt. Express **13**, 267 (2005).
23. J. M. Dudley, G. Genty, and A. S. Coen, Rev. Mod. Phys. **78**, 1135 (2006).
24. G. P. Agrawal, *Nonlinear Fiber Optics* (Academic, 2006).
25. C. Froehly, A. Lacourt, and J. C. Viénot, Nouv. Rev. Opt. **4**, 183 (1973).
26. J. Piasecki, B. Colombeau, M. Vampouille, C. Froehly, and J. A. Arnaud, Appl. Opt. **19**, 3749 (1980).
27. C. Dorrer, J. Opt. Soc. Am. B **16**, 1160 (1999).
28. Since the response time of PD1 (~500 ps) is much longer than the pulse duration (~100 fs), the measured signal, i.e., the convolution of both functions, is equal to the PD1 response function scaled by a factor proportional to the pulse energy.
29. S. H. Strogatz, *Nonlinear Dynamics and Chaos* (Perseus Books, 1994).